Interaction of hot carriers with optical phonons in Selenium

A. Darbandi, O. Rubel *

Thunder Bay Regional Research Institute, 290 Munro St, Thunder Bay, Ontario, Canada
Lakehead University, 955 Oliver Road, Thunder Bay, Ontario, Canada

A B S T R A C T

An interaction of hot charge carriers with optical phonons in Selenium is studied theoretically from first principles. The results suggest that the electron–phonon matrix element for energetic electrons is significantly greater than that for holes. This effect is attributed to the weak coupling of lone-pair states to lattice perturbations associated with optical vibrational modes. Hence, the energy relaxation time due to the emission of optical phonons for holes is expected to be longer than that for electrons. The longer relaxation time favors the impact ionization of holes.

© 2011 Elsevier B.V. All rights reserved.

1. Introduction

The interest in amorphous chalcogenide semiconductors, specifically amorphous Selenium (a-Se), experiences a renaissance due to a unique combination of its photoconducting properties and a feasibility of impact ionization at practical electric fields [1–3] making a-Se a promising functional material for photosensors. Emerging applications include TV camera tubes that are capable of capturing images at extremely low light intensities [2,4], X-ray detectors [5,6], and γ-ray detectors [7] for medical imaging.

Presently, the practical aspects of avalanche in a-Se are better understood than the theoretical side. The main puzzle was to explain how a primary charge carrier can gain the kinetic energy of several electron-volts in the low-mobility semiconductor, where the carrier mean free path is of the order of interatomic spacing. The controversy was resolved by introducing two scattering mechanisms (elastic due to disorder and inelastic due to optical phonons) in the framework of a modified lucky-drift model [4,8,9]. The mobility is then governed by elastic scattering on a disorder potential, while the scattering by optical phonons is responsible for the energy relaxation. The model provides a reasonable fit to the experimental data on a field dependence of the impact ionization coefficient in a-Se [4,9–11]. However, the phenomenological nature of the model provides no insight to the magnitude of the mean free paths, which are treated as free parameters. Also, it is still unclear, what makes a-Se a unique disordered semiconductor that features impact ionization at practical electric fields? Why do holes undergo avalanche at lower fields than electrons [12]? The purpose of this communication is to uncover these questions.

In this paper we will investigate the interaction of charge carriers with optical phonons in Selenium by calculating the corresponding matrix element from first principles. Our results suggest that the square of the absolute value of the matrix element for electrons is by an order of magnitude greater than that for holes. This result is attributed to the weak coupling of lone-pair states to perturbations associated with optical vibrational modes and interpreted along the line of a simple tight-binding model proposed in Ref. [13]. Since the scattering rate is proportional to the square of the corresponding matrix element, the energy relaxation time due to the emission of optical phonons for holes is expected to be longer than that for electrons.

2. Calculations of matrix elements of electron–phonon interaction

The calculations were performed for trigonal Selenium (t-Se) assuming that the obtained results are also applicable to the amorphous phase. This choice is supported by X-ray ultraviolet and inverse photoemission measurements [14–16] that reveal an almost identical density of states in amorphous and trigonal Selenium. The phonon density of states for amorphous and crystalline phases are also identical, except for a relative shift of the optical branch by approximately 3 meV [17], which is not crucial for the purpose of our study. These similarities are likely due to this fact that the amorphous structure is similar to the crystalline one on a short-range scale.

Despite these similarities, the transport properties of crystalline and amorphous phase are drastically different. The highest value for the hole mobility in a-Se is about 1 $cm^2 v^{-1} s^{-1}$ [18], whereas the hole mobility in trigonal Selenium is in the range of 10–40 $cm^2 v^{-1} s^{-1}$ [19–21]. This difference is attributed to the intensive elastic scattering

Table 1

Phonon frequencies at Γ-point and lattice parameters of t-Se obtained theoretically using DFT with two different approximations (LDA and GGA) for the exchange correlation functional.

	Optical phonon frequency (cm^{-1})				Lattice parameters (Å)		
	A1	A2	E1	E2	a = b	c	ρ
Experimental	237[a]	103[a]	233[a]	144[a]	4.366[b]	4.953[b]	1.86[b]
					4.277[c]	4.974[c]	
GGA	230	84	218	126	4.544	5.055	1.88
LDA	...	...	...	...	3.879	5.080	1.89

[a] Nakayama [32].
[b] Room-temperature data [33].
[c] Results of the measurements are extrapolated to $T = 0$ K [34].

by a disorder potential in the amorphous structure. However, a part of the mobility that is controlled by electron–phonon interactions is the same for amorphous and crystalline state of the material (see Ref. [22, p. 2]). Therefore, results of our calculations for the electron–phonon interaction in trigonal Selenium can also be translated to its amorphous phase.

The structure of t-Se consists of parallel helical chains arranged with a hexagonal symmetry and characterized by two lattice constants a, c and the radius of the chain ρ (see Table 1). Calculations of the electron–phonon matrix elements were performed in the framework of density functional theory (DFT) implemented in the `ABINIT` package [23,24] using planewave method and Troullier–Martins pseudopotential [25]. The full structural optimization was performed using two approximations for the exchange correlation functional: local (LDA) and generalized density (GGA) approximations. Convergence tests were performed with respect to the k-mesh density and the plane wave cutoff energy E_{cut}. The convergence was reached at $E_{cut} = 25$ Ha and $4 \times 4 \times 4$ Monkhorst-Pack k-point mesh [26]. The theoretical values of the structure parameters are listed in Table 1. The GGA results show a superior agreement with the experimental structural parameters. Therefore, GGA was chosen for further calculations of the matrix elements.

The matrix element is defined as

$$G_{m \to n}^{\tau, \alpha}(\mathbf{k} \to \mathbf{k} + \mathbf{q}) = \langle \psi_{n, \mathbf{k}+\mathbf{q}} \left| \frac{\partial V_e}{\partial \mathbf{r}_{\tau, \alpha}} \right| \psi_{m, \mathbf{k}} \rangle, \quad (1)$$

where $\psi_{m, \mathbf{k}}$ and $\psi_{n, \mathbf{k}+\mathbf{q}}$ are the electron wave function associated with the initial and final states, respectively, m and n are the band indexes, $\mathbf{k}$ and $\mathbf{q}$ are the electron and phonon wave vectors, respectively, and $\partial V_e / \partial \mathbf{r}_{\tau, \alpha}$ is the derivative of the electron potential energy with respect to the displacement of atom τ in the direction α [27].

The matrix elements were calculated explicitly for nine perturbations (three atoms and three directions) using a response function technique implemented in `ABINIT` [28].

3. Results

The unit cell of t-Se consists of three atoms, leading to a total of nine phonon branches: three acoustical and six optical [29,30]. The optical phonon frequencies of t-Se obtained by solving a secular equation at Γ-point are listed in Table 1 along with experimental data for comparison. Only four optical modes are listed in Table 1 because of the degeneracy. The calculated frequencies are in agreement with the experimental values, which gives a confidence in our structural model.

In the following we focus the attention on modes A1 and E1. These two modes are expected to play a major role in the energy relaxation of hot carriers in Selenium, since they both have the highest energy and the highest density of phonon states [17]. Fig. 1 illustrates A1 and E1 modes. The A1 mode is the so-called breathing mode that corresponds to the atomic displacements in x–y plane. The E1 mode is associated with atomic displacements along the chain (Fig. 1b). Next, we perform the calculations of matrix elements for these two modes.

The general set of matrix elements G defined by Eq. (1) is atom- and direction-specific (τ and α). The phonon-specific matrix element is obtained by combining G with eigenvectors $\mathbf{u}_l^\tau(\mathbf{q})$ that determine the amplitude of atomic vibrations for the mode l [27]

$$M_{l, m \to n}(\mathbf{k} \to \mathbf{k} + \mathbf{q}) = \sum_\tau \mathbf{u}_l^\tau(\mathbf{q}) \cdot \mathbf{G}_{m \to n}^\tau(\mathbf{k} \to \mathbf{k} + \mathbf{q}), \quad (2)$$

Our preliminary study is limited to the relaxation that involves small q-vectors, which corresponds to energy relaxation of charge carriers, but not their momentum. This assumption allows us to eliminate a complex integration in q-space. The energy conservation is enforced by considering only diagonal elements, i.e. $M_{l, m \to m}$.

The band structure of t-Se is shown in Fig. 2a along with the matrix elements at high-symmetry points of the Brillouin zone for A1 and E1 phonon modes. The data are shown in 2 eV range of excess energy for electrons and holes, since the minimum excess energy of a charge carrier required to ionize the electron–hole pair is about the energy gap [31]. The results in Fig. 2a show that the absolute values of the square of matrix elements in the valence band are by an order of magnitude lower than that in the conduction band. This indicated that electrons show a stronger coupling to phonon perturbations than holes.

Fig. 2a shows only a general trend for a limited selection of high symmetry k-points. More representative data can be obtained by performing the calculation on a denser mesh of 64 k-points with further averaging for each band taking into account the weight of individual

a

b
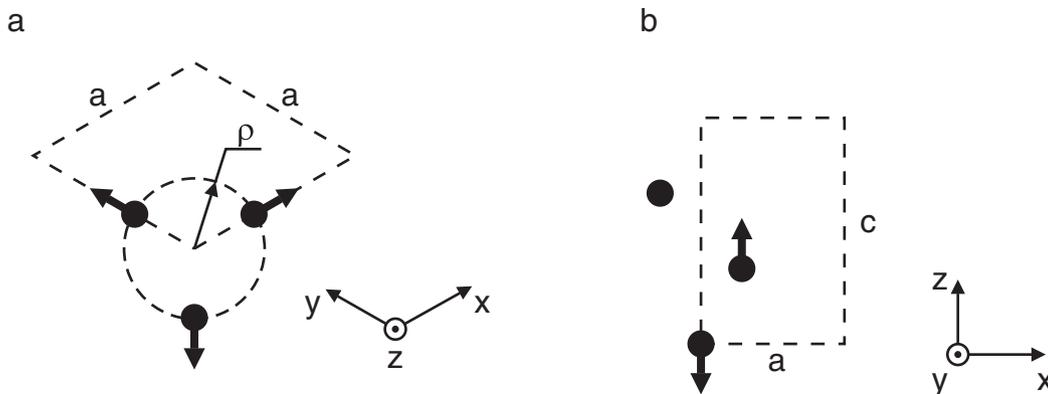
Fig. 1. High-energy optical phonon modes in t-Se. A1 and E1 modes are shown on panels (a) and (b), respectively.
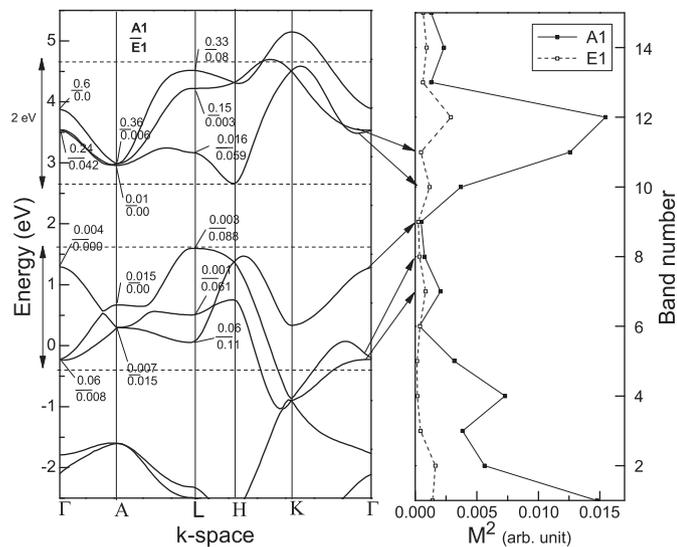
Fig. 2. Band structure (a) and the square of the optical phonon matrix element (b) for t-Se. Values in the numerator and denominator on panel (a) correspond to the matrix element squared for *A*1 and *E*1 modes, respectively.

k-points. The corresponding band-average squared matrix elements are shown in Fig. 2b.

4. Discussion

The bands 7–9 in Fig. 2b correspond to the top of the valence bands, so-called lone pair-states, and the bands 10–12 are the bottom of the conduction band. The square of matrix elements in the conduction band is by an order of magnitude greater than that for the top of the valence band. Since the scattering rate is proportional to the square of the corresponding matrix element, the energy relaxation time due to the emission of optical phonons for holes will be longer than that for electrons. This result correlates with the experimental observation that holes undergo avalanche at lower electric fields than electrons [12].

Furthermore, one can see that the absolute value of square of the matrix element increases with an increase of the excess energy of holes and electrons (Fig. 2b). Similar observations were made for an acoustical phonon deformation potential [13]. The weak response of upper valence states to lattice perturbation has been attributed to the fact that the lone-pair states are not involved in hybridization, as opposed to the states in the conduction band [13].

5. Conclusion

Calculation of electron–phonon matrix elements in trigonal Selenium was performed for optical phonon modes. The calculation results suggest that energetic holes should experience a weaker interaction with optical phonons than electrons. The results for holes are attributed to the weak interaction of lone-pair states with the corresponding phonon modes and linked to the favorable high-field transport of holes in amorphous Selenium.

References

[1] G. Juska, K. Arlauskas, Phys. Status Solidi (a) 59 (1980) 389.
[2] K. Tanioka, J. Yamazaki, K. Shidara, K. Taketoshi, S. Kawamura, T. Shioka, Y. Takasaki, IEEE Electron Device Lett. 8 (1987) 392.
[3] K. Tsuji, Y. Takasaki, T. Hirai, K. Taketoshi, J. Non-Cryst. Solids 114 (1989) 94.
[4] S. Kasap, J.A. Rowlands, S.D. Baranovskii, K. Tanioka, J. Appl. Phys. 96 (2004) 2037.
[5] C. Dylan, S. Hunt, Kirby, J. Rowlands, Med. Phys. 29 (2002) 2464.
[6] W. Zhao, D. Li, A. Reznik, B. Lui, D. Hunt, J. Rowlands, Y. Ohkawa, K. Tanioka, Med. Phys. 32 (2005) 2954.
[7] S. Kasap, J. Frey, G. Belev, O. Tousignant, H. Mani, L. Laperriere, A. Reznik, J. Rowlands, Phys. Status Solidi (b) 246 (2009) 1794.
[8] O. Rubel, S. Baranovskii, I. Zvyagin, P. Thomas, S. Kasap, Phys. Status Solidi (c) 1 (2004) 1186.
[9] O. Rubel, A. Potvin, D. Laughton, J. Phys. Condens. Matter 23 (2011) 055802 [7 pp.].
[10] A. Reznik, S. Baranovskii, O. Rubel, G. Juska, S. Kasap, Y. Ohkawa, K. Tanioka, J. Rowlands, J. Appl. Phys. 102 (2007) 053711.
[11] K. Jandieri, O. Rubel, S. Baranovskii, A. Reznik, J. Rowlands, S. Kasap, J. Mater. Sci. Mater. Electron. 20 (2009) S221.
[12] G. Juska, K. Arlauskas, Phys. Status Solidi (a) 77 (1983) 387.
[13] O. Rubel, D. Laughton, J. Phys. Condens. Matter 22 (2010) 355803.
[14] N. Shevchik, J. Tejeda, M. Cardona, D.W. Langer, Solid State Commun. 12 (1973) 1285.
[15] N. Shevchik, M. Cardona, J. Tejeda, Phys. Rev. B 8 (1973) 2833.
[16] I. Ono, P.C. Grekos, T. Kouchi, M. Nakatake, M. Tamura, S. Hosokawa, H. Namatame, M. Taniguchi, J. Phys. Condens. Matter 8 (1996) 7249.
[17] F. Gompf, J. Phys. Chem. Solids 42 (1981) 539.
[18] G. Juska, J. Non-Cryst. Solids 137 (1991) 401.
[19] D. Qin, H. Tao, Y. Zhao, L. Lan, K. Chan, Y. Cao, Nanotechnology 19 (2008) 355201.
[20] V. Bogomolov, V. Poborchii, S. Kholodkevich, JETP Lett. 31 (1980) 436.
[21] B. Gates, B. Mayers, B. Cattle, Y. Xia, Adv. Funct. Mater. 12 (2002) 219.
[22] A. Rose, Electron Phonon Interaction, World Scientific, 1989.
[23] X. Gonze, B. Amadon, P.M. Anglade, J.M. Beuken, F. Bottin, P. Boulanger, F. Bruneval, D. Caliste, R. Caracas, M. Cote, T. Deutsch, L. Genovese, Ph. Ghosez, M. Giantomassi, S. Goedecker, D.R. Hamann, P. Hermet, F. Jollet, G. Jomard, Lero, Comput. Phys. Commun. 180 (2009) 2582.
[24] X. Gonze, Kristallograhie 220 (2005) 558.
[25] M. Fuchs, Comput. Phys. Commun. 119 (1999) 67.
[26] H. Monkhorst, J. Pack, Phys. Rev. B 13 (1976) 5188.
[27] F. Murhpy-Armando, S. Fahy, Phys. Rev. B 78 (2008) 035202.
[28] C. Lee, X. Gonze, Phys. Rev. B 51 (1995) 8610.
[29] W. Teuchert, R. Geick, Phys. Status Solidi (b) 61 (1974) 123.
[30] W. Teuchert, R. Geick, G. Landwehr, H. Wendel, W. Weber, J. Phys. C: Solid State Phys. 8 (1975) 3725.
[31] N. Hindley, J. Non-Cryst. Solids 8–10 (1972) 557.
[32] T. Nakayama, J. Phys. Soc. Jpn. 33 (1972) 12.
[33] H. Swanson, W. Gilfrich, G. Ugrinic, NBS Circular, U.S. GPO, Washington, D.C., 1955, p. 539.
[34] R. Grosse, H. Swoboda, A. Tausend, J. Phys. C: Solid State Phys. 8 (1975) L445.